# Lightweight Force-Controlled Device for Freehand Ultrasound Acquisition

Huayang Sai, Zhenbang Xu, Chengkai Xia, Lijuan Wang, and Jie Zhang

***Abstract*—This study investigates a force-controlled auxiliary device for freehand ultrasound (US) examinations. The designed device allows sonographers to maintain a steady target pressure on the US probe, thereby improving the US image quality and reproducibility. The use of a screw motor to power the device and a Raspberry Pi as the system controller results in a lightweight and portable device, while a screen enhances user-interactivity. Using gravity compensation, error compensation, an adaptive proportional–integral–derivative algorithm, and low-pass signal filtering, the designed device provides highly accurate force control. Several experiments using the developed device, including clinical trials relating to the jugular and superficial femoral veins, validate its utility in ensuring the desired pressure in response to varying environments and prolonged US examinations, enabling low or high pressures to be maintained and lowering the threshold of clinical experience. Moreover, the experimental results show that the designed device effectively relieves the stress on the sonographer's hand joints during US examinations and enables rapid assessment of the tissue elasticity characteristics. With automatic pressure tracking between probe and patient, the proposed device offers potentially significant benefits for the reproducibility and stability of US images and the health of sonographers.**

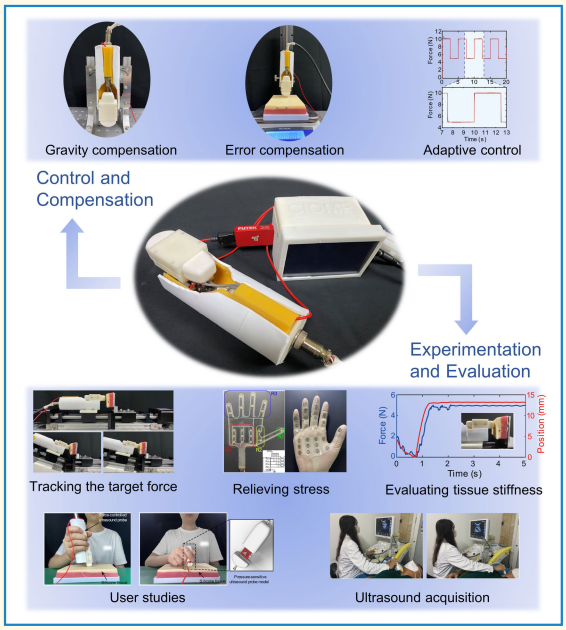


***Index Terms*— Force control, lightweight design, tissue stiffness measurement, ultrasound (US) examination.**

## I. Introduction

AMONG the many medical imaging modalities, ultrasound (US) does not expose sonographers and patients to harmful ionizing radiation, making it the preferred approach for frequent soft tissue imaging. Currently, US imaging plays an important role in numerous medical services, such as fetal imaging [1], thrombosis screening [2], biopsy needle insertion monitoring [3], and skeletal muscle scanning [4]. The safety and versatility of US make it ideally suited to the growing demands on general practitioners. Specifically, the development of auxiliary devices and technologies to improve the diagnostic efficiency and usability of US imaging and healthcare effectively lowers the operational thresholds and experience requirements.

In conventional sonography, the sonographer presses a US probe into a patient's body and applies the necessary pressure to obtain satisfactory US images. Sonographers rely on their experience to make artificial adjustments to the probe pressure based on the interpretation of qualitative US images; thus, variations in the experience level of sonographers may result in significant differences in the diagnostic results. However, the quality of the images is difficult to assess quantitatively. In many developing countries and some medical centers or emergency situations, physicians with this specialized experience may not be available [5], making it challenging to

Manuscript received 12 February 2023; accepted 28 February 2023. Date of publication 3 March 2023; date of current version 29 August 2023. This work was supported in part by the National Natural Science Foundation of China under Grant 11972343. *(Corresponding author: Zhenbang Xu.)*

This work involved human subjects or animals in its research. Approval of all ethical and experimental procedures and protocols was granted by the Ethics Committee of the First Hospital of Jinlin University under Approval No. 2022-426.

Huayang Sai and Chengkai Xia are with the CAS Key Laboratory of On-Orbit Manufacturing and Integration for Space Optics System, Changchun Institute of Optics, Fine Mechanics and Physics, Chinese Academy of Sciences, Changchun 130033, China, and also with the College of Optoelectronics, University of Chinese Academy of Sciences, Beijing 100049, China (e-mail: saihuayang18@mails.ucas.ac.cn; xiachengkai19@mails.ucas.ac.cn).

Zhenbang Xu is with the CAS Key Laboratory of On-Orbit Manufacturing and Integration for Space Optics System, Changchun Institute of Optics, Fine Mechanics and Physics, Chinese Academy of Sciences, Changchun 130033, China (e-mail: xuzhenbang@ciomp.ac.cn).

Lijuan Wang and Jie Zhang are with the Neuroscience Center, Department of Neurology, The First Hospital of Jilin University, Jilin University, Changchun 130021, China (e-mail: wanglj66@jlu.edu.cn; zhangj_0106@jlu.edu.cn).

Digital Object Identifier 10.1109/TUFFC.2023.3252015

***Highlights***

- **A novel force force-controlled device with significant lightweight and portability advantages was developed to assist sonographers in maintaining the probe at the required pressure.**
- **Benefiting from gravity compensation, error compensation, adaptive algorithms, and filtering, the device offers a high level of control accuracy.**
- **Experimental results have shown that the device can assist sonographers in pressure tracking, tissue stiffness assessment, manual stress relief, and enhanced ultrasound imaging.**

obtain accurate and reproducible pressure acquisitions. Even if the structure of the organization remains identical, different contact forces between the probe and tissue can lead to significant differences in US imaging, creating difficulties in accurately reproducing US images. For example, sonographers may be unable to determine whether a tumor has become more prominent over time based on US images because changes in the acquisition status potentially produce misleading variations in appearance. With accurate pressure adjustment, US images taken several months apart can be directly compared with each other, which is valuable in improving the efficiency and accuracy of diagnosis. Therefore, force-controlled systems for US examinations have a wide range of promising applications, as they can be used throughout the human body. By reducing the individualized differences among sonographers, this would enhance the imaging of clinically critical biophysical parameters and improve the reproducibility of imaging results.

In contrast to noncontact computed tomography or magnetic resonance imaging, clinical US examinations require that the probe be placed approximately perpendicular to the tissue surface and in close contact with the skin, with the sonographer maintaining a stable and nearly constant pressure between the probe and tissue. For example, to observe changes in vascular properties such as vessel diameter and flow velocity in subjects before and after drug administration, sonographers are required to maintain a constant force in the probe and tissue for some period of time; otherwise, variations in pressure may cause changes in the muscle tissue and vessel shape, making it difficult to compare the measured indexes [6]. In addition, with the movement of the subject's organs, respiratory effects, and pulsation deformations, especially during prolonged US examinations, the sonographer's hand is prone to involuntary shaking as a result of fatigue, which may lead to significant changes in US images. With premium US systems, sonographers not only operate the US probe but also manipulate a touch panel, trackball, and various buttons of the system with their other hand. Thus, sonographers must have extensive experience and good hand-eye coordination to ensure stable probe pressures. For nonspecialists, this steady pressure requirement is challenging, and an accessible handheld device would be a useful tool to assist them in holding the probe steady on the target tissue for a long time.

Palpation is widely used in clinical medicine, whereby the clinician compares the softness or firmness of the mass to the surrounding tissue by squeezing it. US elastography is a technique for estimating the tissue elastic properties based on US images, i.e., recording the US scan results by applying compression values to the outside of the tissue and processing the data. One of the most important diagnostic applications of tissue impedance measurements is to determine the breast stiffness in subjects using tissue elastography [7], [8], [9], as several studies have shown a potential correlation between the onset and growth of thyroid nodules and tissue stiffness [10]. Although elastography has shown promising applications in clinical diagnosis, it requires a high level of controllable probe pressure. Some research results have shown that, at 10% precompression, the shear wave speed of most soft tissues approximately doubles [11]. Therefore, quantifiable and controllable contact forces contribute to the reliability and reproducibility of elastography results and elicit quantitative measurements based on analysis of the stiffness characteristics.

Prolonged US acquisition increases health risks for sonographers, such as local pain and other musculoskeletal disorders, as they are required to exert large forces on the patient during the imaging procedure [12], [13]. Indeed, 80%–90.5% of sonographers are reported work-related musculoskeletal disorders [14], [15], including bursitis, muscle strains, and peripheral neuropathy of the back [16]. Prolonged US examinations with a probe in hand (20–40 min each) are the most critical factor exacerbating these symptoms [17]. As the demand for diagnostic US applications increases with an aging society, lowering the experience threshold for sonographers and safeguarding the health of US practitioners are urgent issues to be addressed.

In response to the above discussion, this study investigates a lightweight force-controlled auxiliary (LFCA) device for freehand US examinations. The handheld LFCA device automatically maintains the target pressure; therefore, sonographers can focus more attention on the analysis of US images and diagnosis of the condition. Since the LFCA device no longer requires strong operator force control for freehand US, it reduces the requirements for operational experience and significantly improves image reproducibility based on quantifiable pressure data. Furthermore, the relationship between tissue indentation depth and probe pressure can be used to achieve an automated and rapid assessment of the tissue's elastic parameters, which has significant practical implications for clinical diagnosis. Note that a distinctive feature of the LFCA device is its miniaturized and lightweight form, benefiting from ergonomic and user-friendly design considerations that make it easy to use, even for operators with little or no US experience. Therefore, the LFCA device can also be used as a training tool to assist inexperienced sonographers in developing a better intuition for the probe pressure.

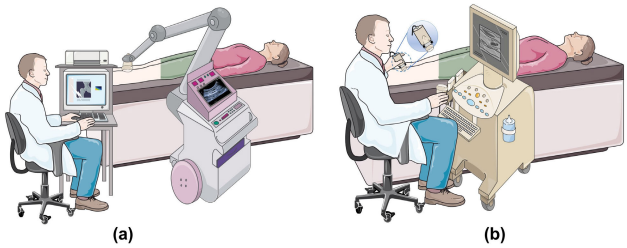


Fig. 1. Two types of devices used to assist in US examinations. (a) Ground-mounted automated US robots. (b) Miniaturized handheld assistive devices.

In the following, we first summarize and highlight the existing relevant technologies. The mechanical and electronic design of the LFCA device is briefly described in Section III, and the compensation and control strategies of the device are introduced in Section IV. Section V presents the results of five experiments to evaluate the performance of the developed device in tracking the target force, relieving the pressure to which the human hand is subjected during US measurements, and determining the ability to identify tissue elasticity characteristics. We analyze the role of the device in enhancing image stability and compensating for the lack of force control capability through a comparative study of two clinical experiments on the human jugular and superficial femoral veins. This article concludes with a discussion of the experimental results, including the advantages and limitations of the proposed device, safety considerations, and directions for future work.

## II. Related Work

The development of devices for enhanced US image acquisition attracted the interest of scholars as early as the 1990s. To the best of our knowledge, Ng et al. [18] were the first to design a transurethral US robot for acquiring prostate images such that the position of the prostate would not change with variations in surgical instruments during the procedure. To date, numerous devices have been developed to assist in US examinations. These can be broadly classified into two categories: ground-mounted automated US robots and miniaturized assistive devices held by the sonographer, as shown in Fig. 1.

Ground-mounted US robotic systems are highly automated but are typically bulky and complex to operate. A significant advantage is that sonographers can operate the device remotely without the need for close contact with the subject, which is an effective method for remote expert clinical diagnosis [19]. For example, Salcudean et al. [20] developed an early US diagnostic robot with a four-bar parallel linkage structure designed for the remote US of the carotid artery. In recent years, benefiting from rapid advances in robotics, several automated US robots have been developed in combination with robotic manipulators for carotid monitoring [21], probe guidance [22], and brachytherapy [23]. Common research themes for automated US acquisition robots include scan path planning, force control, and image quality optimization [24]. At present, most robotic US systems plan autonomous scan paths in a semiautomatic manner [25], [26]. Several systems allow fully automated planned scan paths [27], [28], but this remains a challenging topic. In robotic US systems, the robotic manipulator applies a constant force in the direction normal to the patient's surface [29], [30], [31]. Because the image quality of acoustic propagation is strongly affected by the properties of the medium, some automatic US scanning robots optimize the images by updating the scan path or adjusting the probe in real time [32], [33]. There have been many detailed reviews of robotic US systems [16], [24], [34], [35]. Despite the benefits that US acquisition robotics bring to US consultations, the widespread implementation of robots in treatment facilities is still some way behind the rapid development of industrial robots. The factors hindering the application of US acquisition robots include their excessive size, high cost, safety considerations, and operational complexity.

We believe that handheld semiautomated US auxiliary devices are currently better suited to the demands of US acquisition applications than automated US robots, primarily because they are highly controllable, simple to operate, very safe, and relatively inexpensive. Sonographers hold the auxiliary devices to induce pressure on the probe or to control the probe to produce the desired contact force, thus eliminating the need for scanning path planning and probe posture adjustment. For example, Burcher et al. [36] developed a handheld device that can record the probe position and pressure information, and Schimmoeller et al. [37] designed a handheld device that collects the probe force and orientation while efficiently synchronizing all data to improve the repeatability of the US images. Gilberton and Anthony [38] and Dhyani et al. [39] developed an ergonomic US device that records the probe pressure and torque. However, these devices are only used to record or display pressure information from the US acquisition and cannot automatically compensate for pressure errors. Hence, the adjustment of the probe pressure is still entirely dependent on the sonographer.

Automated handheld US devices typically drive the probe motion with a single degree of freedom. Eura et al. [40] developed a portable US motion compensation device that eliminates the effects of human physiological motion on US images. Marchal and Troccaz [41] designed a force-controlled device that provides feedback to sonographers on the acquired probe pressure using a linear brake, while Nabavizadeh et al. [42] proposed an automated compression device for exerting and maintaining force excitation for a predetermined duration and monitoring the creep response of the tissue to measure the tissue viscosity properties. Wah and Aung [43] designed a handheld force-controlled US probe based on a belt drive and proposed an agent-based sliding mode control method with added friction compensation to ensure the overdamped response of the system. Scholars at the Massachusetts Institute of Technology (MIT) have researched US devices for several years, resulting in three generations of handheld force-controlled US devices that allow sonographers to apply stable pressure to the patient [44], [45], [46], [47] and evaluate Duchenne muscular dystrophy [48]. All three generations use a ball screw linear brake to convert the servo motor's rotational motion to the probe's linear motion, offering the advantages of small size and high control accuracy.

Although a variety of handheld force-controlled US devices have been developed, they suffer from the following shortcomings. First, most existing handheld devices are not conducive to prolonged operation by sonographers. For example, the handheld device proposed in [40] is large and requires sonographers to operate it by lifting. Marchal and Troccaz [41], Gilbertson and B. Anthony [47], and Rivaz and Rohling [49] presented devices that are too long to allow practical operation by sonographers. Although Koppaka et al. [46] and Gilbertson [50] considered ergonomics in their third-generation handheld force-controlled US probe, the design of the motor and screw slide results in a mass of 850 g, which is not conducive to prolonged holding. Therefore, there is a need for handheld force-controlled US devices that are smaller, lighter, and easier to hold. This is essential for relieving joint pains in sonographers' hands during prolonged US examinations. Second, although some handheld force-controlled US devices have been designed to be small, they typically rely on an external computer to perform the interaction [38], [44], [51], which leads to an overall lack of portability and increases the cost burden. Our previous work [6] developed a much smaller device using a programmable logic controller and an interactively operable screen, but this still has a large mass. Third, although some devices have considered gravity compensation [44], [45], [46], the torque and friction are often neglected, which leads to the collected probe pressure being different from the actual pressure applied. In consideration of the abovementioned problems with existing handheld devices, this article describes the design, use, and analysis of a lightweight, low-cost, and high-accuracy LFCA device.

## III. Force-Controlled US Device: Mechanical and Electrical Designs

In this section, we briefly describe the mechanical design, electronics, and software of the proposed handheld force-controlled US device.

### A. Mechanical Design

To reduce the mass of the device, a small screw motor (K25, Yingpeng Aircraft Power, Shenzhen, China) provides the power source, with a miniature force sensor (LSB201, FUTEK, Irvine, CA, USA) mounted at the end of the screw to collect the pressure of the probe (see Fig. 2). The force sensor is bolted to a 3-D-printed mounting clip and connector, the lower end of which is bolted to a slider on the rail. To prevent the movement of the motor from exceeding the travel limit, two proximity switch sensors (M4 NPN, LUOSHIDA, Dongguan, China) provide position information through a shading piece fixed to the connector. The proximity switch sensor is triggered once the slider approaches the movement limit of the device, allowing a maximum movement of 25 mm. The device is equipped with an angle sensor (MPU6050, INVENSENSE, Sunnyvale, CA, USA) to measure its inclination and enable gravity compensation, which is described in detail in Section IV-A. The designed device can be adapted to different types of probes by simply replacing the probe clamp of the device.

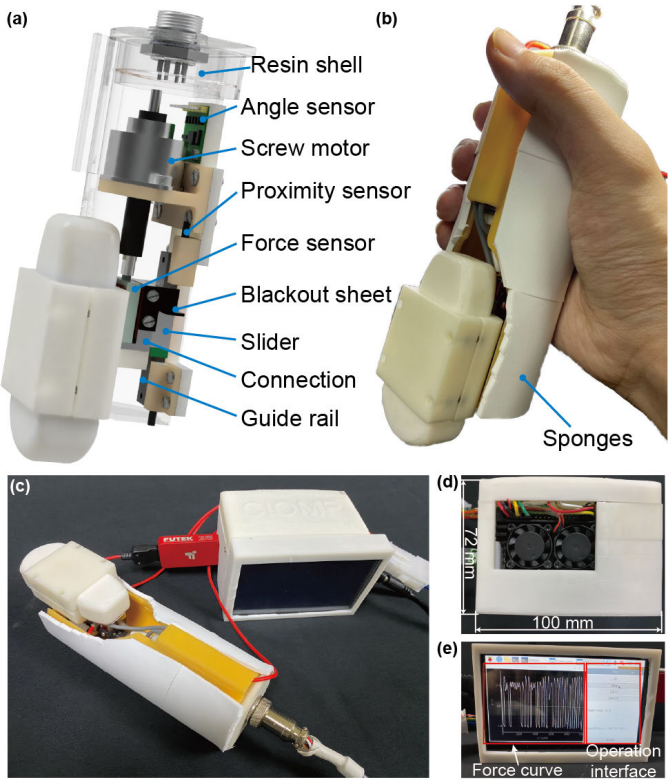


Fig. 2. Design of the force-controlled US device. (a) Rendering of the handheld device. (b) Physical view of the handheld device. (c) Force-controlled US device including the handheld device and controller. (d) Back view of the controller. (e) Front view of the controller and the operation interface.

A 3-D-printed resin housing with an approximately oval cross section protects the operator's hand from moving parts and is designed in consideration of people's gripping habits. The resin shell is wrapped in a layer of sponge to reduce the pressure on the operator's hand and the discomfort that may be caused by the vibration of the motor, and the noise generated in use does not exceed 60 dB. The size of the housing is 46 mm × 51 mm × 140 mm, and the total mass of the handheld device is 287 g, including 54 g of the US probe. To the best of our knowledge, the designed device is lighter than all existing force-controlled devices for freehand US examinations.

### B. Electronic and Software Design

The lightweight controller contributes to the portability of the device and to its widespread applicability. The designed controller is shown in Fig. 2(d) and (e), and has a volume of 69 mm × 100 mm × 72 mm and a total mass of 493 g. The controller shell is 3-D-printed from resin material and includes an integrated Raspberry Pi development board, a stepper motor driver, a 5-in DSI display, and two fans for heat dissipation.

The central controller for the LFCA device is a Raspberry Pi 4 Model B (Raspberry Pi Foundation, Cambridge, U.K.). This has the advantages of small size, developability, and expandability. The pressure error is transmitted as an input signal to the designed adaptive proportional–integral–derivative (PID) controller, and the output signal is transmitted to the

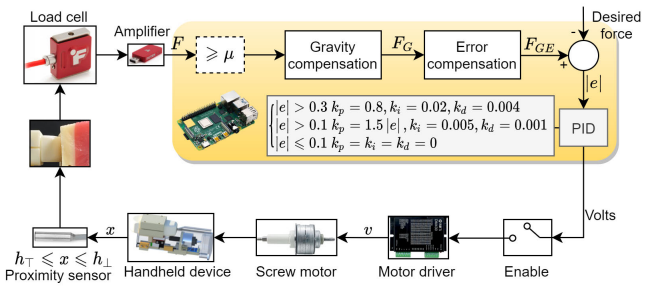


Fig. 3. Block diagram of the closed-loop control signal. The yellow area indicates the processing of the collected force signal by the main controller, and the dashed box is executed only once.

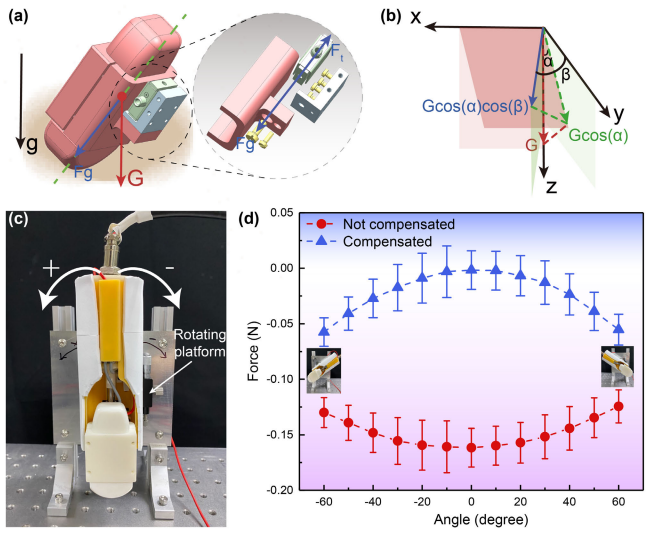


Fig. 4. Gravity compensation of the LFCA device. (a) Schematic of the force sensor assembly, where the gravity component indicated in red affects the force measurements. (b) Relationship between gravity and tilt angle. (c) Experimental setup for device angle adjustment. The LFCA device is mounted on a precision rotating stage, with counterclockwise rotation noted as a positive angle and clockwise rotation as a negative angle. (d) Average and standard deviation of the force sensor before and after gravity compensation over the range −60° to 60°. Dots represent mean forces, while the error bars indicate the standard deviation obtained from five trials.

stepper motor driver (DM430, Yingpeng Aircraft Power), which drives the screw motor to execute the drive command. The control signaling flow is shown in Fig. 3. We set a small startup threshold of $\mu = 2$, i.e., and send the motor motion command when the pressure error is larger than the set threshold after the operator starts the force tracking command. The driver first controls the screw motor to position the slider at the end stroke position. This is because it is often difficult to operate the controller while simultaneously placing the probe on the human site to be inspected, and there is a possibility that the slider will be at the forward position of the stroke at startup, which may cause the probe to reach the limit of travel before attaining the desired pressure. During the movement of the motor, the proximity sensors constantly detect whether the probe has reached its limit position. Once the proximity sensor has been triggered, further movement of the motor is disabled to prevent the travel limit of the probe from being exceeded.

The interactive interface is based on the Python graphical user interface. As shown in Fig. 2(e), operators can start, stop, and adjust the desired pressure directly from the interface through a 5-in DSI display without any external device. The developed operating system enables the fast startup to ensure that the device is available in real time, and the interface can display the evolution of the probe pressure. All control parameters are integrated into the controller and do not require setting by the operator. As a result, the sonographer can independently operate the LFCA device following a simple introduction, removing the high learning cost of operating multijoint robotic manipulators.

## IV. Control and Compensation

In this section, we first describe the gravity and error compensation of the LFCA device. The aim of these compensation techniques is to ensure accurate measurement of the probe pressure by the force sensor. The force control scheme of the device is then designed, and low-pass filtering is considered as a means of denoising the pressure signal.

### A. Gravity Compensation

The gravity of the probe and probe clamp can cause a pull on the force sensor, which will affect the accuracy of the collected pressure data. When sonographers perform US examinations, the probe is not always directed vertically downward but may be inclined against the detection surface, as shown in Fig. 4(a). Since the pressure error caused by the gravity of the probe is highly related to its inclination angle, we can effectively compensate for the error of the device according to the collected inclination angle of the probe. The part to be compensated can be considered as the gravity $G$, and so a coordinate system is established with its origin at the center of mass, as shown in Fig. 4(b). The rotation of the device along the $z$-axis direction does not affect the force sensor, so only the rotation angles of the probe along the $x$-axis and the $y$-axis are considered. Assuming that the probe is rotated by angles of $\alpha$ and $\beta$ about the $x$- and $y$-axes, respectively, the component of the total gravitational force $G$ along the direction of the force sensor is $G\cos(\alpha)\cos(\beta)$. Therefore, the probe pressure after gravity compensation can be expressed as

$$F_G = F_{\text{sen}} + G\cos(\alpha)\cos(\beta) \tag{1}$$

where $F_{\text{sen}}$ denotes the value measured by the force sensor. The rotation angles $\alpha$ and $\beta$ can be detected by the angle sensor mounted on the LFCA device. $G$ can be determined by the force sensor when the probe is oriented vertically downward and without any contact.

An experimental setup in which the rotation angle can be precisely varied was designed to evaluate the gravity compensation effect of the LFCA device, as shown in Fig. 4(c). The values reported by the force sensor before and after gravity compensation were recorded at 5° intervals over the test range of −60° to 60°, with five tests performed at each angle. The experimental results are shown in Fig. 4(d). Because the probe

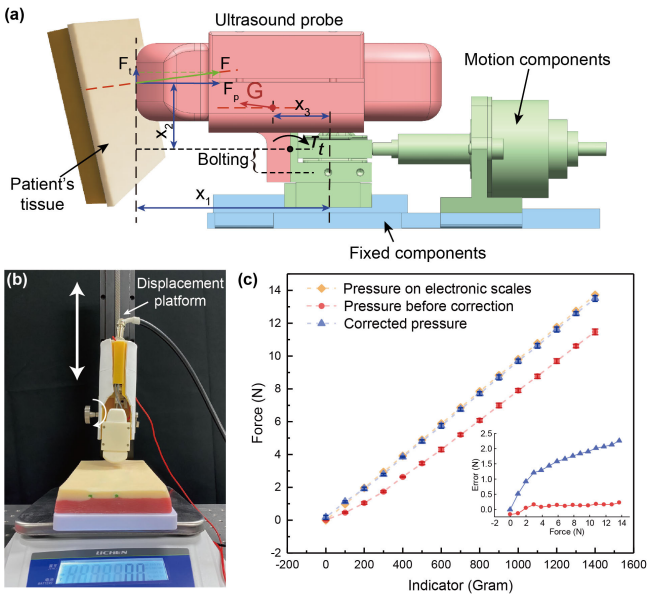


Fig. 5. Error compensation of the LFCA device. (a) Schematic of the forces on the device when in contact with tissue, where the components of the same color can be considered collectively. (b) Experimental device for testing the actual pressure applied to the probe. After the silicone tissue is placed onto the electronic balance, the electronic balance is calibrated to zero. The probe is then pressed against the tissue by controlling the vertical moving platform until the electronic balance displays the desired weight, and the value of the force sensor is noted. (c) Pressure values collected before and after compensation. The pressure on the electronic balance is calculated as $F = mg$, where $m$ is the weight collected by the electronic balance and $g = 9.8$ m/s$^2$ is the acceleration of gravity.

is not subjected to any pressure, the desired force should remain at 0 N. The results show that the force sensor measures between $-0.125$ and $-0.175$ N before gravity compensation and between 0 and $-0.06$ N after compensation, which demonstrates that the measurement accuracy is significantly improved by the gravity compensation technique. As the angle of tilt increases, the compensated error gradually increases, mainly as a result of the gradual increase in the angle sensor error as the angle increases.

## B. Error Compensation

Other factors besides gravity will impact the tracking accuracy of the device, such as the force sensor being affected by torque, and these factors can be affected by the actual pressure of the probe independent of the tilt angle of the device. As shown in Fig. 5(a), owing to the irregular probe shape and cable, the probe cannot be installed on the same axis as the force direction of the sensor, so it is located at a distance of $x_2$ from the force sensor. When the probe is exposed to an actual pressure $F$, part of the pressure is converted into torque components of $F_t x_1$ and $F_p x_2$. Note that extended strokes require larger values of $x_1$, resulting in larger torques on the force sensor [6], [45]. Although much of the torque can be offset by the construction of the device, the collected pressure data may be significantly affected by friction and the assembly precision, resulting in a sensor pressure that is less than the actual pressure of the probe. To compensate for the pressure error, we designed the experimental setup shown in Fig. 5(b) so that the rotation angle of the device is always kept to zero. Based on the MATLAB fitting of a large amount of experimental data, the pressure on the probe after error compensation can be expressed as

$$F_{GE} = F_G + 0.8614|F_G|^{0.3524}. \tag{2}$$

Subsequently, pressure values were collected from 0 to 1400 g at 100-g intervals before and after compensating for the pressure, with five tests performed at each pressure value. As shown in Fig. 5(c), the probe pressure collected by the force sensor is always smaller than the actual pressure of the probe prior to error compensation, and the error increases with increasing probe pressure. After compensation, the collected pressure value is broadly consistent with the actual pressure on the probe. When the pressure on the probe is close to 14 N, the pressure errors before and after compensation are 2.25 and 0.22 N, respectively, representing an error reduction of 90.2%. This demonstrates that the LFCA device with error compensation provides accurate feedback on the pressure to which the probe is subjected, laying the foundation for accurate tracking of the desired pressure.

## C. Force Control

A simplified system model is shown in Fig. 6(a). The LFCA device is held against the patient by the sonographer. The position of the device held by the sonographer is denoted as $x_1$, the end position of the probe is $x_2$, and the interface in contact with the patient is denoted as $x_3$. The probe is driven by a screw motor to produce a displacement of $\Delta x$, so the position of the probe $x_2$ can be expressed as

$$x_2 = x_1 + \Delta x. \tag{3}$$

The position of the screw motor can be expressed as

$$\Delta x = \frac{K_A u(t)}{M_p} \times l \tag{4}$$

where $K_A$ denotes the gain constant, $u(t)$ is the output value of the controller, $M_p$ denotes the number of pulses set by the motor driver, and $l = 1$ mm denotes the pitch of the motor screw. Note that the maximum movement speed of the screw is limited to 17.5 mm/s to ensure the safety of the patient.

Two separate controllers were developed and tested. Taking the simplest approach first, we applied a PID control law, similar to that for the position controller

$$e(t) = F_{\text{ref}}(t) - F_{\text{sen}}(t) \tag{5}$$

$$u(t) = k_p e(t) + k_i \int_0^t e(t) + k_d \frac{\mathrm{d}e(t)}{\mathrm{d}t} \tag{6}$$

where $F_{\text{ref}}(t)$ denotes the desired force, $F_{\text{sen}}(t)$ denotes the measured force from the force sensor, $e(t)$ denotes the force error, and $k_p, k_i$, and $k_d$ are the proportional, integral, and derivative control gains, respectively.

According to the impedance relationship, the actual contact force $F_{\text{act}}$ between the probe and the patient's interface can be expressed as

$$F_{\text{act}} = K(x_2 - x_3) + B(\dot{x}_2 - \dot{x}_3) \tag{7}$$

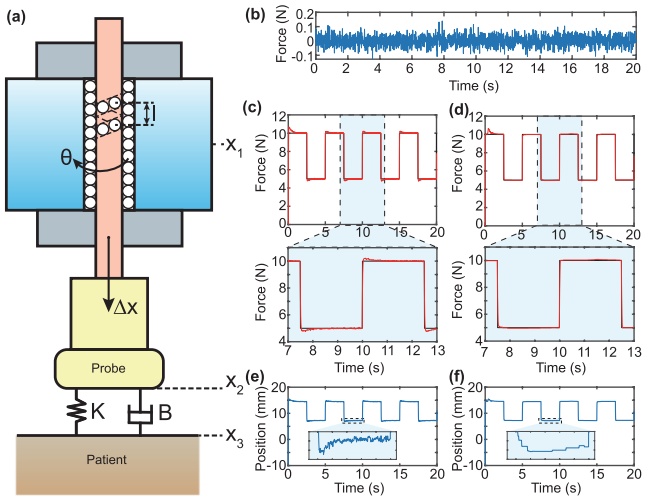


Fig. 6. Modeling and simulation of the LFCA device. (a) System model of the device in contact with the patient. (b) Disturbance added to the force sensor. (c) Actual tracking force of the system with the PID controller. (d) Actual tracking force of the system with the adaptive PID controller. (e) Position of the probe with the PID controller. (f) Position of the probe with the adaptive PID controller.

where $K$ and $B$ denote the stiffness and damping of the patient's body. The measured force $F_{\text{sen}}(t)$ can be expressed as

$$F_{\text{sen}}(t) = F_{\text{act}}(t) + F_{\text{dis}}(t) \tag{8}$$

where $F_{\text{dis}}(t)$ denotes the noise disturbance on the sensor.

We assume that the initial conditions of the system are $x_1 = -0.1$, $\Delta x(0) = x_3 = 0$. According to Wood et al. [52] and Speich et al. [53], the stiffness values range from 40 to 44 000 N/m and the damping values from 3.6 to 175 Ns/m, with large differences in stiffness between skeletal and soft tissues. Considering the silicone tissue used in our experiments, the impedance parameters were chosen as $K = 690$ N/m and $B = 10$ Ns/m, respectively. In combination with the pulse count of the motor drive, $K_A$ and $M_p$ are set to $K_A = M_p = 4000$. Through experience and repeated trials, the control parameters can be set as $k_p = 0.8$, $k_i = 0.02$, and $k_d = 0.004$. Consider a random disturbance, as shown in Fig. 6(b). The simulation results in Fig. 6(c) and (e) show that there is an overshoot in the pressure tracking of the probe, and the probe position is in a continuously chattering state.

Next, the PID controller was modified, and an adaptive PID controller was designed as

$$\begin{cases} |e| \geqslant 0.3 \;\; k_p = 0.8, k_i = 0.02, k_d = 0.004 \\ |e| > 0.1 \;\; k_p = 1.5|e|, k_i = 0.005, k_d = 0.001 \\ |e| \leqslant 0.1 \;\; k_p = k_i = k_d = 0. \end{cases} \tag{9}$$

When the force error satisfies $|e| < 0.3$, a smaller set of control parameters is considered to prevent the tracking pressure from overshooting, thus ensuring the safety of the patient. For practical US examinations, an error of 0.1 N does not affect the US images of in vivo tissues, such as the gastrointestinal wall [54]. Therefore, when the force error satisfies $|e| < 0.1$, the continuous chattering is alleviated by stopping the motion of the motor. As shown in Fig. 6(d) and (f), the tracking pressure does not overshoot when using the adaptive PID controller. Moreover, the chattering frequency of the probe is significantly reduced, which is beneficial for improving the life of the motor. A theoretical analysis of the stability of this adaptive PID control method is beyond the scope of this article, but, in practice, it remains quite stable, even under high-frequency operation. It is worth mentioning that, different from the control strategy that processes the acquired US image to adjust the position of the probe, the designed device achieves a faster adjustment frequency of the probe by analyzing the probe pressure, which allows the LFCA device to cope with complex changes in human or patient position.

### D. Steady-State Performance and Filtering

Using the proposed adaptive PID controller, we tested the steady-state tracking performance of the LFCA device in a static environment. The requirement was to achieve fast tracking from an initial noncontact situation to a desired force of 2 N. The experimental process is shown in Fig. 7(a). The tested tissue is soft silicone that can be used to simulate areas such as the human breast or abdomen. The results of five experiments are recorded in Fig. 7(c), showing that the device can achieve fast and accurate tracking of the desired pressure.

Because the pressure signal collected by the force sensor contains numerical noise, a set of denoising steps must be applied to the collected force data. Referring to the steps for denoising a data signal in [29], the pressure corresponding to the probe motion is mainly distributed in the low-frequency range because of the high-frequency sampling of the force sensor ($F_s = 100$ Hz) and the low-speed linear motion of the probe ($\leqslant 17.5$ mm/s). Therefore, a low-pass filter is used to suppress the high-frequency noise in the system, with a fast Fourier transform (FFT) applied to determine its stopband frequency. The FFT results of the measured force and the corresponding power spectral density (PSD) are shown in Fig. 7(b). As the PSD decays rapidly after 5 Hz, the stopband frequency of the low-pass filter can be set to this value. However, the application of a low-pass filter leads to a constant phase shift (group delay), i.e., a time delay $t_{\text{de}}$, which is defined as the derivative of the phase with respect to the frequency [55]. The time delay $t_{\text{de}}$ can be corrected by shifting the denoised signal further. For a general S-tap low-pass filter, $t_{\text{de}}$ can be calculated by

$$t_{\text{de}} = (S-1)/(2 * F_s). \tag{10}$$

The average values of the filtered and corrected forces from the five tests are compared with the untreated data in Fig. 7(c).

Furthermore, the transient performance of the LFCA device was tested. After the contact force between the probe and tissue had stabilized at 2 N, multiple step changes in the measured force of the system were achieved by increasing the target force by 1 N every 5 s until the target force reached 5 N. As shown in Fig. 7(d), the system exhibits an overdamped response with no overshoot. The average rise time is 0.1 s (10%–90%), and the average steady-state error is +0.076 N (+7.6%). Therefore, the LFCA device achieves accurate tracking of different target pressures with good transient performance.

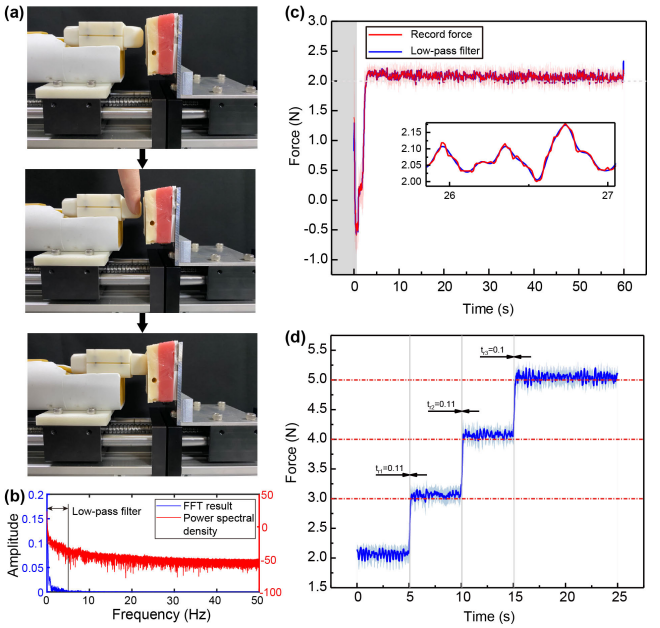


Fig. 7. Filtering and step response of the LFCA device. (a) Experimental process of tracking the target force. After starting the force control and setting the desired force, the handheld device automatically tracks the force after the probe is touched by a finger. (b) FFT results and PSD. (c) Comparison of force values and unprocessed data before and after filtering and correction for tracking a target force of 2 N, where the gray region indicates the force change during the probe retraction to the end position after the finger has touched the probe, and the red translucent region indicates the standard error. (d) Force values during the sequential steps of the device from a target force of 2–5 N. The blue curve indicates the average force value of the five tracking tests, the translucent blue region indicates the standard deviation, the translucent gray region indicates the rise time area, and the red dashed line indicates the target force value.

## V. Experiments

This section describes five experiments conducted to evaluate the performance of the designed LFCA device and its advantages in US examinations. The local ethics committee has approved the experiments, and informed consent was obtained from all participants.

### A. Tracking the Target Force in Dynamic Situations

In US examinations, neither the US probe nor the patient's detection site will remain stationary, and tissue movements may be caused by physiological behaviors, such as the patient breathing or the unconscious shaking of the sonographer's hand. As shown in Fig. 8, the designed LFCA device and soft silicone tissue were fixed on two screw slides to simulate the motion of the tissue and changes in the probe position.

In this experiment, force tracking was considered for silicone tissue or the device moving at different speeds and for the silicone tissue and the device moving together. In the first set of experiments, the silicone tissue was subjected to reciprocal motion with an amplitude of 5 mm at 1, 2, and 3 mm/s; the test was repeated five times at each speed. The experimental results and the variation in the silicone position with time are shown in Fig. 8(b)–(e). The device obtains a smaller tracking error at lower motion speeds. Even with the maximum motion speed, the error is less than 0.6 N, which allows for stable

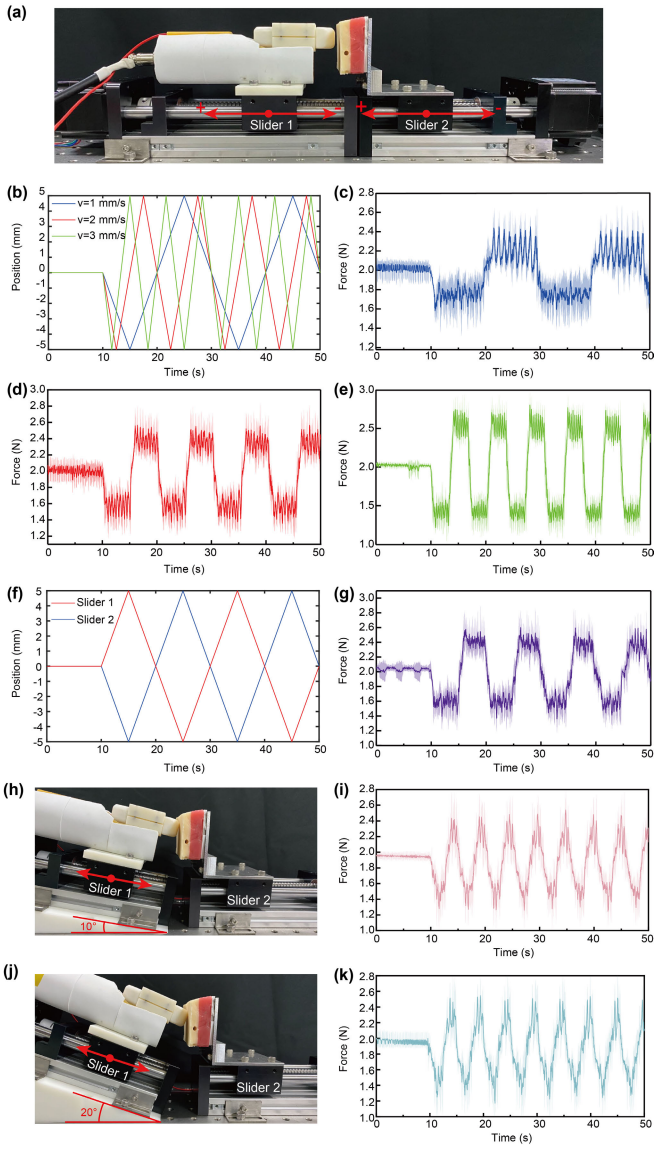


Fig. 8. Force tracking of the LFCA device in dynamic situations. (a) LFCA device and soft silicone tissue fixed to the sliders of two screw slides, where the positive and negative signs indicate the direction of slider movement. (b) Displacement curves of slider 2 moving at 1, 2, and 3 mm/s. (c)–(e) Average pressure curves in five tests with slider 2 moving at 1, 2, and 3 mm/s, respectively. (f) Displacement curves for the simultaneous motion of sliders 1 and 2 at a speed of 1 mm/s. (g) Average pressure curve of the probe during five tests with both sliders moving simultaneously. (h) Device is at a 10° angle to the vertical plane of the tissue. (i) Average pressure curves in five tests with 10° angle and slider 1 moving at 2 mm/s. (j) Device is at a 20° angle to the vertical plane of the tissue. (k) Average pressure curves in five tests with 20° angle and slider 1 moving at 2 mm/s. The translucent region indicates the standard error.

US images to be obtained. In the second set of experiments, the device and silicone tissue were reciprocated at a speed of 1 mm/s, as shown in Fig. 8(f). The tests were performed five times, and the experimental results are shown in Fig. 8(g). Even if the probe and silicone tissue move reciprocally, the maximum tracking error is still less than 0.6 N, and the device can respond quickly to external changes. In the third set of experiments, we set the deflection angle between the device and the vertical plane of the tissue to 10° and 20°, respectively,

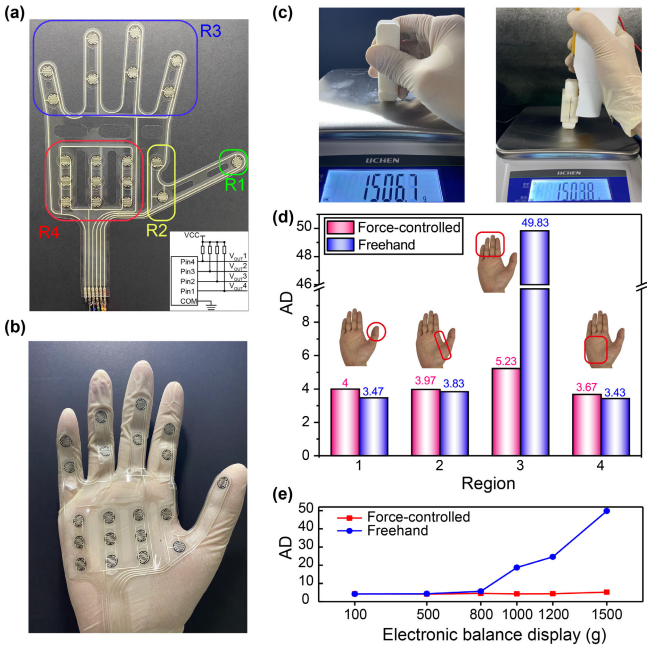


Fig. 9. Comparison of the pressure applied to various regions of the human hand using a flexible thin-film pressure sensor. (a) Hand-shaped flexible thin-film pressure sensor and its circuit diagram, where R1–R4 indicate the four pressure regions. (b) Flexible thin-film pressure sensor attached to a rubber glove. (c) Flexible thin-film pressure sensor collecting AD values of each region with the probe and device pressed on the electronic balance. (d) Average AD values for each region collected by the flexible thin-film pressure sensor for 30 s. (e) Maximum average AD value at different target pressure values.

and silicone tissue was subjected to reciprocal motion with an amplitude of 2.5 mm at 2 mm/s. The experimental results are shown in Fig. 8(i) and (k) for five tests at each tilt angle, respectively. The test results show that the different inclination angles between the device and the tissue do not affect the pressure-tracking performance of the device, and an error range of ±0.6 N can still be guaranteed in a situation where the position of the device is constantly changing. Therefore, the designed LFCA device can be used to assist sonographers in overcoming involuntary hand movements and changes in the position of the tissue being measured by maintaining a stable target force.

### B. LFCA Device for Relieving Stress on the Hand

US auxiliary devices should be held manually to relieve the stress on the hand joints during prolonged US examinations. In this experiment, we evaluated the effect of using the LFCA device on relieving the stress on the operator's hand joints compared with using the US probe freehand. As shown in Fig. 9(a) and (b), a flexible thin-film pressure sensor in the shape of a human hand was designed to collect the pressure on four regions of the operator's hand. The operator held a probe model with and without the LFCA device against the electronic balance and was required to maintain a pressure of around 1500 g (14.7 N) for 30 s, as shown in Fig. 9(c). The analog–digital (AD) value collected by the thin-film pressure sensor can be compared directly to the pressure applied to the human hand. With a sampling frequency of 1 Hz, the average AD value for each region was calculated. As shown in Fig. 9(d), when the designed LFCA device is used for pressure acquisition, the pressure on region 3 is significantly lower than that with the freehand US probe, and the pressure on the other regions is only slightly larger than in the case of freehand US. This is because of the small size and irregular shape of the probe, which requires the operator to perform the US examination in a pinching manner, concentrating the pressure on the index knuckles. Therefore, the designed device significantly alleviates the pressure on individual areas of the hand by spreading the pressure, as the shell better conforms to the shape of the hand.

Furthermore, we considered the effectiveness of the LFCA device in performing US examinations at different target pressures to relieve manual stress. Separate averages were collected for the operator at different target pressures for 30 s, and we found that the hand was constantly subjected to the highest average pressure in region 3. As shown in Fig. 9(e), when the electronic balance is subjected to a force of less than 800 g (about 7.84 N), there is no significant difference between the maximum pressure suffered by the hand with and without the LFCA device. When the pressure applied by the probe is greater than 800 g, the maximum pressure on the operator's hand with the freehand US probe increases rapidly. In contrast, the pressure on the hand does not change significantly when using the LFCA device, implying that the designed device has a more significant effect on relieving the pressure in region 3 of the hand when used for US examinations with high target pressures. Furthermore, optimizing the device's shell with ergonomics and finite element simulation can further reduce the pressure on the human hand.

### C. LFCA Device for Evaluating Tissue Stiffness Parameters

The relationship between the displacement of the tissue and the pressure allows the impedance parameters of the tissue to be effectively estimated. A stiffness parameter measurement program was developed to assess the stiffness characteristics of the tissue. When the US probe was in contact with the tissue at any pressure, the probe was rapidly backed off until the pressure reached zero. A target force of 5 N was then immediately tracked, and the position of the probe and the pressure change curve were recorded. The human tissue can be represented by the following linear mass–spring–damper impedance relationship [56]:

$$F(t) = M\frac{\mathrm{d}^2x(t)}{\mathrm{d}t^2} + B\frac{\mathrm{d}x(t)}{\mathrm{d}t} + Kx(t) \tag{11}$$

where $F(t)$ is the pressure on the probe and $x(t)$ is the displacement of the probe. The impedance parameters $M$, $B$, and $K$ denote the inertia, damping, and stiffness properties of the tissue, respectively. Based on the relationship between the collected pressure $F(t)$ and the position $x(t)$, $K$ can be obtained by parameter fitting through the Levenberg–Marquardt algorithm.

We selected tissues with three different elasticity characteristics for the estimation of stiffness parameters, as shown in Fig. 10(a). The soft silicone, hard silicone, and medium

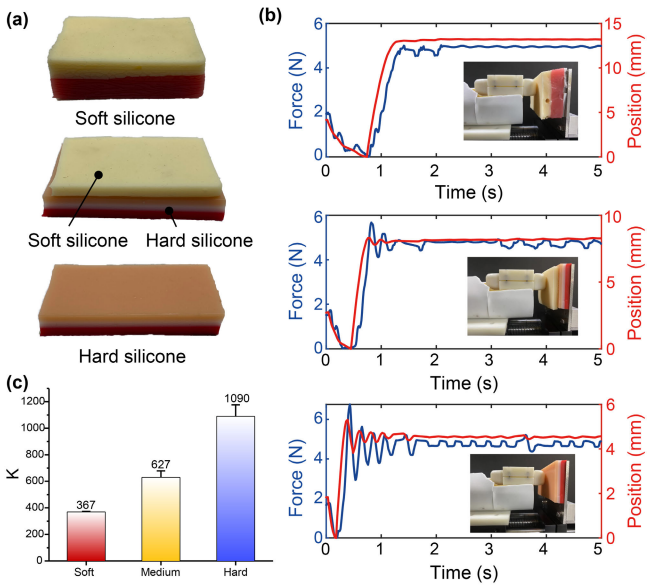


Fig. 10. LFCA device for stiffness parameter estimation. (a) Three silicone tissues with different stiffness characteristics. (b) Average position and average pressure profile of the probe over three tests on each tissue type using the LFCA device. (c) Mean values of the stiffness parameter $K$ measured in the three tests and their standard errors.

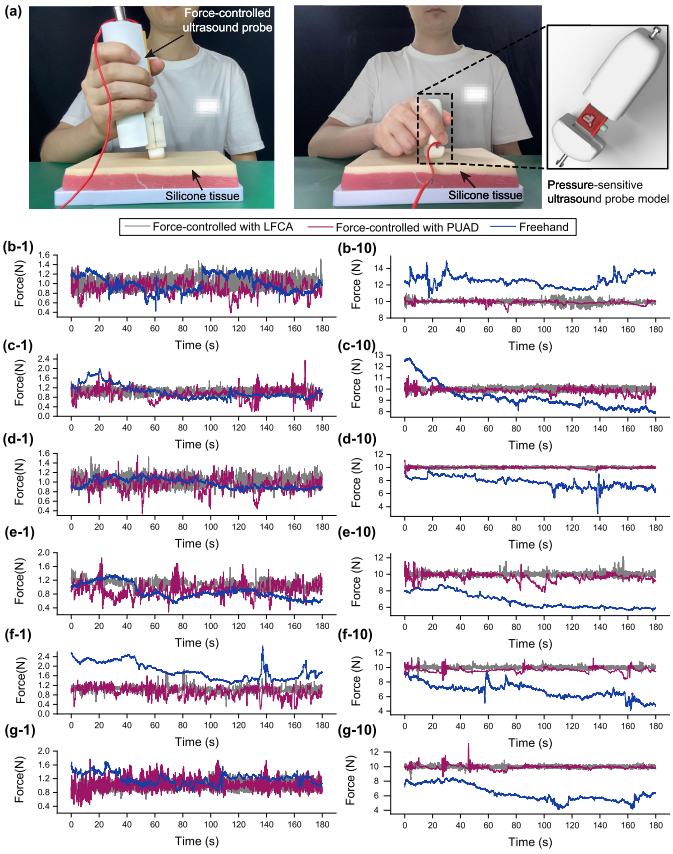


Fig. 11. Force-controlled devices and freehand US for tests on maintaining a target force. (a) Operator maintaining the target force using the LFCA device, PUAD, and the freehand US, respectively. For the freehand US, the operator used a probe model with an embeddable force sensor. (b)–(g) Pressure profiles of six operators over 3 min, where (b)–(d) correspond to three experienced sonographers and (e)–(g) correspond to three volunteers with no experience in US examinations. The numbers 1 and 10 indicate the target force.

silicone (a combination of the soft and hard types) were each tested three times using the LFCA device. The average values of the probe position and pressure with respect to time are shown in Fig. 10(b). The stiffness characteristics of the tissues obtained by fitting are shown in Fig. 10(c). The hardness characteristics of the different tissues are compatible with their actual hardness. Therefore, the designed LFCA device can quickly and efficiently measure the stiffness characteristics of human tissues, making it suitable for the early screening of diseased tissue areas. A numerical comparison with the stiffness characteristics of healthy tissues can then be performed, reducing the need for sonographers to have extensive force control experience.

### *D. LFCA Device Enabling Operators to Maintain the Target Force*

Achieving stable tracking of the target force over a period of time is one of the most important functions of the LFCA device. Following Gilbertson and Anthony [45], [47], who performed user studies to evaluate the performance of a device in a realistic imaging scenario, we conducted a user study to clarify the performance of the designed LFCA device. In contrast to previous studies, and considering the wide range of applications of US examinations, the target force was varied according to the detection scenario. For example, US imaging of superficial venous vessels requires a small probe pressure, while vessels under thick fat require a large probe pressure. Therefore, we tested two different pressure values in this experiment and performed a statistical analysis. We considered not only the stationary state but also the performance of the device during US scanning. In this section, freehand US refers to the operator directly holding the probe for the examination, whereas force control refers to the operator using the designed LFCA device and previous portable ultrasonic auxiliary device (PUAD) [6]. To avoid confusion, in this article, the test results using PUAD will be stated; otherwise, the one used is the LFCA device designed in this work.

Six operators performed pressure tests for 3 min with target forces of 1 and 10 N using the LFCA device and a freehand probe model that can record pressure, as shown in Fig. 11(a). Three of the six operators were sonographers with more than one year of experience in clinical US, and the other three were volunteers with no experience in clinical US. For the force-controlled scenario, the operators used the LFCA device and the PUAD for pressure testing after the controller had set the target force. For the freehand US scenario, the operators were first asked to perform a 30-s force perception test by observing the collected pressure values. This was followed immediately by them relying on their memory of this pressure perception to maintain the target pressure. The collected pressure values in both schemes could not be observed by the operators during the pressure collection process.

The experimental results are shown in Fig. 11(b)–(g). First, for the target force of 1 N, the error when using the designed LFCA device is in the range of $\pm 0.2$ N. There are large differences in the pressure curves corresponding to the various

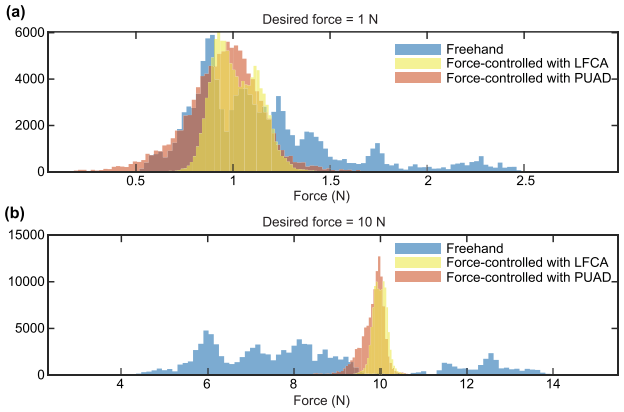


Fig. 12. Histograms of forces applied by all six operators in two test scenarios. (a) Target force of 1 N. (b) Target force of 10 N.

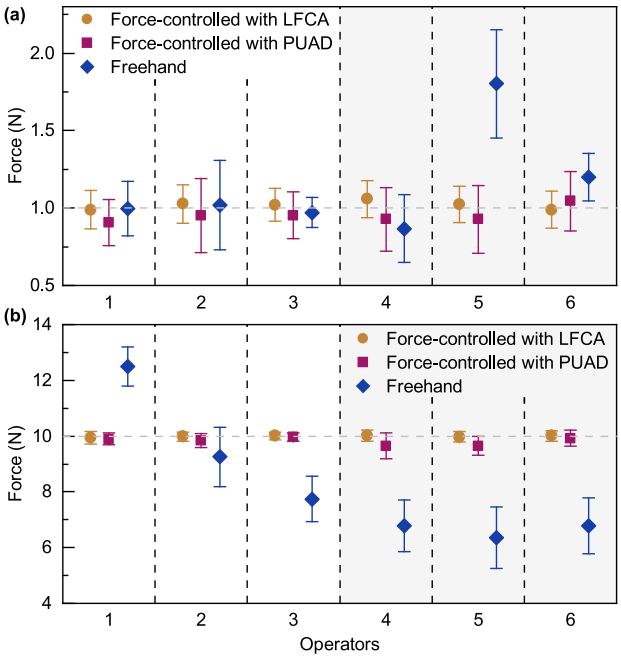


Fig. 13. Mean values and standard errors of forces in two scenarios for six operators. (a) Target force of 1 N. (b) Target force of 10 N. The gray regions indicate the inexperienced operators, the dots indicate the average force collected over 3 min, and the vertical bars indicate the standard error.

operators in the freehand operation scenario, especially for inexperienced operators (e) and (f), who produced large deviations in pressure tracking with time. For a target force of 10 N, the pressure using the proposed device remains stable at around 10 N throughout the test, with little change over time. However, for the freehand operation scheme, except for experienced operator (b), whose pressure curve does not vary significantly, the pressure curves of all other operators exhibit a significant decreasing trend over time. This is caused by the operator's hand joints being subjected to large pressures and the gradual decrease in force perception from the gradual fatigue of the hand muscles over time. In addition, with a small target force, the operators require little additional pressure above the mass of the probe itself, so they can easily maintain a memorized target force at the beginning of the operation. However, it is more difficult to accurately remember a large target force, even for experienced sonographers. That is, the human hand often has a poor capacity for force memory and force perception. Therefore, it may be difficult for sonographers to apply repeated forces to the same tissue without assistance from external conditions. Moreover, the margin of error between the probe pressure and the desired pressure obtained with the LFCA device is smaller than that obtained with the previous PUAD, and operators expressed less fatigue after testing with the LFCA device, especially during the desired pressure of 1 N.

Fig. 12 shows histograms of the force values recorded for all operators in both scenarios. The force-controlled scenario produces a more centralized shape with respect to the target force than freehand operation. Moreover, in the freehand operation with a 1-N target force, the experimental results show that the collected force values are more likely to be greater than the target force. In contrast, with the 10-N target force, the data from the freehand operation show a significantly smaller bias toward the target force. It is also obvious that the pressure distribution results obtained with the LFCA device are more concentrated on the desired value compared to the PUAD, which is consistent with the above analysis.

Fig. 13 shows the mean force and the standard error of the six operators using the devices and freehand collection in the two test scenarios. Experienced operators obtain average force values closer to the target force in the freehand scenario, which implies that experienced sonographers generally have better force perception. Moreover, the mean force and target force values are significantly closer to the desired force values under the force-controlled scenario than under the freehand scenario, with little difference in the test results between operators with different levels of experience. This conclusion is more evident for the target force of 10 N. The standard error of the force in the freehand scenario is significantly higher than when using the LFCA device at a target force of 10 N, indicating that the force applied in freehand operation fluctuates more significantly. Meanwhile, the standard error obtained by almost all operators using PUAD is larger than that of the designed LFCA device at a target force of 1 N. This means that the LFCA device can assist the sonographer to get more stable US images in the clinic.

Furthermore, statistical analysis was performed in the R computing environment (version 4.1.2, R Core Team, 2019) to illustrate the statistical significance of the test results. We used a multivariate permutation analysis of variance (PERMANOVA) with the "adonis" function to examine the differences in the experimental data under three factors (target pressure: 1 N/10 N, forced-controlled/freehand, and experienced/inexperienced). The analysis results are shown in Fig. 14. There is no obvious difference between the results using the LFCA device and the freehand probe at a target force of 1 N. However, at the target force of 10 N, the force control with the LFCA device and the freehand operation show significant differences at the level of $P < 0.05$, and the operators' experience in freehand operation leads to significant differences in the test results at $P < 0.05$. At a target pressure

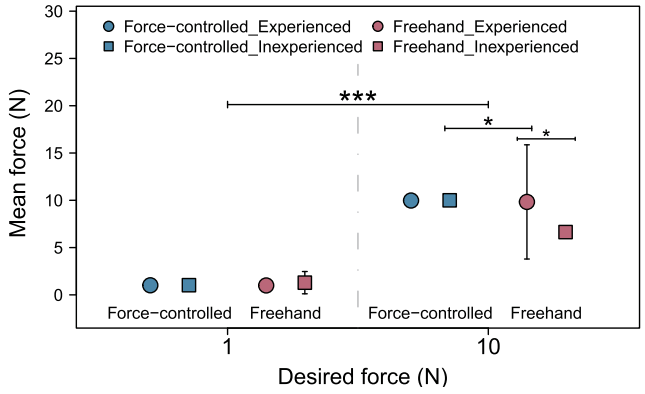


Fig. 14. Differences in the force-controlled and freehand operation of the required pressure values in tests conducted by experienced and inexperienced operators. The error bars represent the standard error. *: $P < 0.05$, **: $P < 0.01$, and ***: $P < 0.001$.

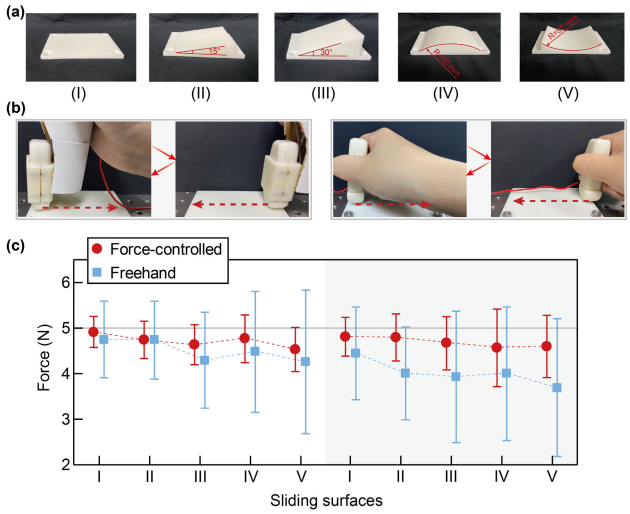


Fig. 15. LFCA device and freehand for US scanning tests. (a) Five different sliding surfaces fabricated by 3-D printing. (b) Operators performed one reciprocal scan on each sliding surface using the LFCA device and freehand. (c) Mean and standard error of scans performed by three experienced sonographers and three inexperienced volunteers on different sliding surfaces using the LFCA device and freehand, where the gray regions indicate the inexperienced operators.

of 10 N, the test results of experienced sonographers are closer to the desired pressure value than those of inexperienced operators, but there are significant variations in the test results between sonographers. In contrast, differences in experience do not lead to significant differences in test results in the force control tests, implying that the LFCA device reduces the level of expertise required to obtain reproducible US images.

In some clinical diagnoses, sonographers are required to perform US scans over large regions of the body, rather than in fixed positions, such as US scans of the human spine [57]. However, the breathing of the patient and the undulations of the human back [58] make it challenging to maintain stable pressure during the scan. Therefore, we evaluated the LFCA-based device and freehand scanning of different shapes of surfaces, thus demonstrating the effect of the device in improving probe pressure stability in US scanning.

As shown in Fig. 15(a), five different sliding surfaces were designed. Six operators used the LFCA device and freehand probe to perform one reciprocal scan with the probe perpendicular to the sliding surface at a speed of approximately 10 mm/s with a target force of 5 N. Three of the six operators were experienced sonographers, and the other three were volunteers with no US-related experience. The experimental results in Fig. 15(c) show no obvious differences over the different scanning surfaces in the force-controlled scenario. Both the mean and standard error of the force-controlled scan results have significantly smaller deviations than in the freehand scenario. Comparing the experimental results of the different operators shows that experienced sonographers can always obtain more accurate pressure results in freehand operation. The average pressure results of freehand operation tend to be smaller than the desired value, mainly because of the operator's tendency to relax the pressure on the probe when reversing the scanning direction. This bias is especially evident for larger inclinations and surfaces, such as cases III–V. Moreover, compared with the experimental results in Fig. 13, the larger stiffness factor of the sliding surface produces a large standard error, and the probe pressure is more likely to fluctuate during the scan. It can be concluded that US scanning with the LFCA device achieves significantly better performance than freehand scanning, and the operator's experience exhibits relatively little influence.

### E. LFCA Device for US Examination of the Jugular and Superficial Femoral Veins

There are two common operational requirements in US examinations. For jugular vessels, sonographers are required to ensure sufficient integrity to provide a view of the vessel flow velocity and diameter, which often requires slight pressure to be applied. For superficial femoral veins, sonographers are required to apply considerable pressure to observe the presence of thrombosis by compressing the superficial femoral vein until it is closed. Therefore, in this experiment, we performed clinical experiments on the human jugular and superficial femoral veins using the LFCA device and freehand. The experimental results allow us to assess the performance of the designed device in clinical applications.

Four operators participated in this experiment, namely, three sonographers with five, two, and one years of experience, respectively, and one volunteer with no clinical US experience. As shown in Fig. 16, the operators performed a 30-s US examination of the jugular and superficial femoral veins of one subject using the LFCA device and freehand, respectively. The subject was an adult male, 27 years of age, in good health. The Doppler US system (HI VISION Ascendus, Hitachi Aloka Medical Ltd., Tokyo, Japan) with a 5–13-MHz linear array transducer was used. To evaluate the US imaging quality, the image frames of the recorded video were first binarized. Compressed vessels show as white in the binarized image (gray value of 1); noncompressed vessels show as black (gray value of 0). The ratio of white pixel points to the total number of pixel points in the intercepted valid region gives the compression index $\lambda_c$, and the ratio of black pixel points to the total number of pixel points gives the uncompressed index

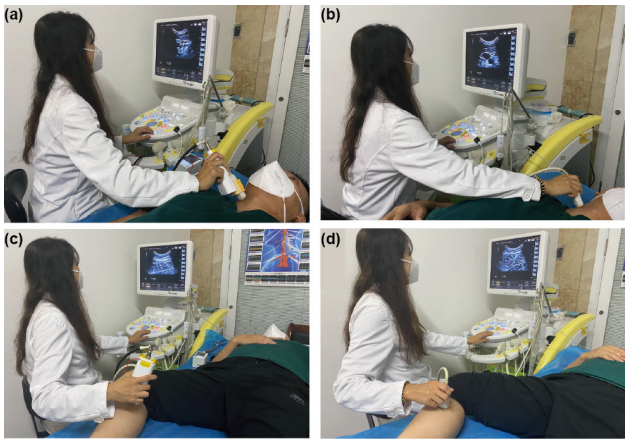


Fig. 16. Operator performing US examinations on the subject's jugular and superficial femoral veins. (a) and (b) Volunteers performing US examinations of the subject's jugular vein using the LFCA device and freehand. (c) and (d) Volunteers performing US examinations of the superficial femoral vein using the LFCA device and freehand.

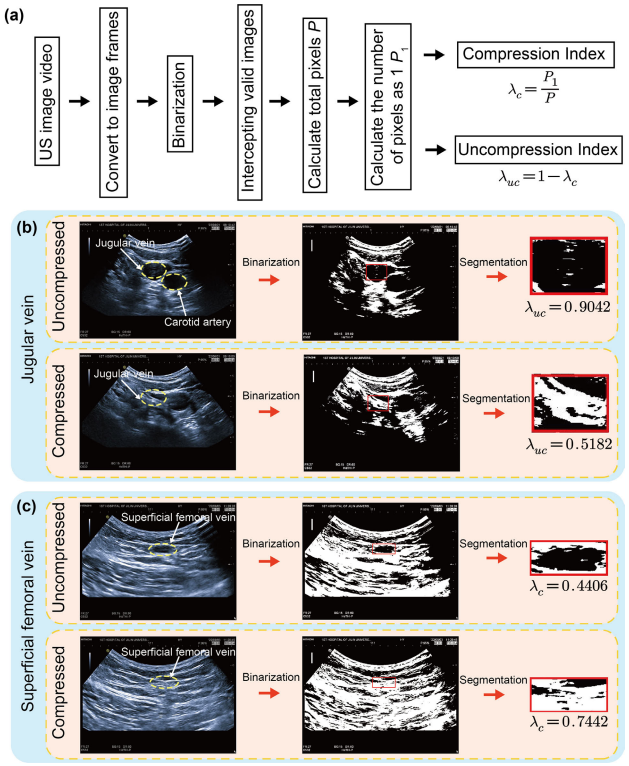


Fig. 17. US image processing. (a) Process of calculating compressed and uncompressed indices based on US examination video. (b) Typical uncompressed versus compressed image analysis in jugular vein US. (c) Typical uncompressed versus compressed image analysis in superficial femoral vein US.

$\lambda_{uc}$. The image processing results are shown in Fig. 16(a). The image effects of the jugular and superficial femoral veins are evaluated using $\lambda_{uc}$ and $\lambda_c$, respectively. For the jugular and superficial femoral veins, larger values of $\lambda_{uc}$ and $\lambda_c$ indicate better US image performance. Fig. 17(b) and (c) shows the status of the compressed and uncompressed vessels in the US examination of the jugular and superficial femoral veins and the calculation process of the evaluation index.

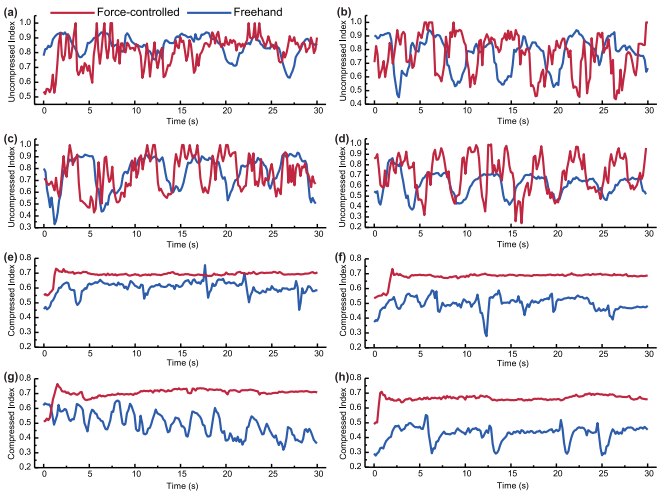


Fig. 18. US results for the jugular and superficial femoral veins produced by operators with different levels of experience. (a)–(d) Uncompressed rate over time for jugular vein US examinations performed by operators with five, two, one, and zero years of experience. (e)–(h) Uncompressed rate over time for superficial femoral vein US examinations performed by operators with five, two, one, and zero years of experience.

The experimental results in Fig. 18 show that the uncompressed index of the jugular vein fluctuates, which is mainly because of the vasoconstriction and dilatation caused by the respiratory effect of the subject. When the jugular vessels are compressed, it causes restricted vasodilation, resulting in a significant reduction in the peak of the acquired uncompressed rate, as shown by the freehand results in Fig. 18(d). In the jugular vein US, the LFCA device appears to be unremarkable in enhancing the uncompressed rate of the vessel for experienced operators. However, for the inexperienced operator [see Fig. 18(d)], the uncompressed rate of the jugular vein is noticeably improved by the LFCA device, and the results are no longer significantly different from those of the experienced operators. Since the position of the probe is constantly being adjusted in small increments when using the force-controlled device, there are more pronounced small fluctuations in the test results, which can be mitigated by increasing the value of 0.1 in the adaptive PID controller (9). In Fig. 18(e)–(h), the compression rate of the superficial femoral vein is significantly improved by the LFCA device for operators with less than five years of experience. The compression rate does not fluctuate significantly over time, implying that the superficial femoral vein is always compressed.

Histograms of the uncompressed and compressed rates for all operators are shown in Fig. 19. The uncompressed rate of 1 in Fig. 19(a) occurs when US images cannot be detected after the complete detachment of the US probe from the subject when using the LFCA device. Generally, although the LFCA device does not significantly improve the jugular vein US, the compression of the superficial femoral vein is concentrated at around 0.7, indicating the fully compressed state and significantly improved US examination performance. Moreover, in the US examination of the superficial femoral vein, the compression index using the LFCA device barely changes with time, except at the initial moment, which means

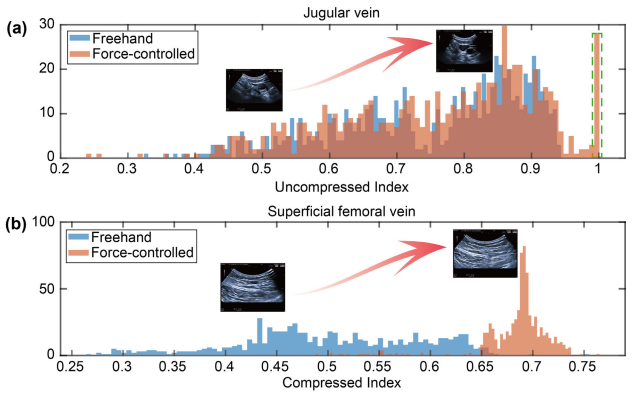


Fig. 19. Histograms of the compression and uncompressed indices in jugular and superficial femoral vein US. (a) Histogram of the uncompressed index of the jugular vein. (b) Histogram of the compression index in the superficial femoral vein.

that the stability of the US image has been significantly improved.

In practical US, sonographers are required to diagnose the patient based on analysis of the US images, but operators must also focus on pressure control in the case of freehand US. When using the LFCA device, the pressure between the probe and the subject is mainly regulated by the device. Therefore, analysis of the US images does not affect the results, which means that sonographers can focus on the diagnosis of the patient's condition rather than on the pressure of the probe.

## VI. Discussion and Future Work

In this section, we highlight the significance of the designed LFCA device in clinical US and experiments, and compare its performance with several representative freehand US devices. The limitations of the designed device, safety aspects, and future work are also discussed.

### A. Applications and Comparisons

As the development of technology continues, US is becoming increasingly intelligent, with one of the most fundamental goals being to achieve quantifiability and controllability. This work has developed a lightweight handheld device that assists sonographers by actively controlling the probe pressure during US examinations. The performance of the designed device has been evaluated in terms of the mechanical design, the software design, and the control system. Several experimental results show that the designed device has a significant effect on the rapid acquisition of tissue elasticity characteristics, relieving stress on sonographers' hand joints, maintaining a stable target force for a long time, and improving the reproducibility of US images. Based on a comparison of its use by operators with different levels of experience, the designed device can be easily used by inexperienced operators and significantly improves their performance. Therefore, it can be inferred that the designed device can be used to develop force perception capabilities in physicians lacking relevant experience, helping to overcome the lack of US specialists in remote areas. Wide application of US technology, lack of competitive similar products, and no modification to the existing equipment, contribute to a broad market prospect for the designed device. However, the key challenge to be considered in the commercial rollout is how to change the operating habits formed by sonographers over the years.

Although the idea of using handheld devices to assist sonographers in US examinations was proposed by scholars two decades ago, there have been few reports on such devices. Those devices that have been developed have limited practical applicability because of problems including their weight, interactivity, and cost. The device described in this article largely overcomes these constraints, paving the way for the clinical application of US-assisted devices through a more comprehensive consideration of device design and experiments. Several experimental results are of value for the future development of US-assisted devices. For example, the pressure on a sonographer's hand was quantified for the first time by a flexible thin-film pressure sensor. Researchers in the development of related devices and developers of US probes can evaluate the comfort of the device similarly and focus on pressure alleviation in hand region 3. For the first time, we have extended the traditional handheld US device beyond a single aspect. Based on the evaluation of elastic parameters, the proposed LFCA device can rapidly measure the elastic parameters of human tissue, providing an alternative to nonlinear elastography for the evaluation of breast tumors [8]. Compared to the conventional method of estimating tissue stiffness by elastography, the designed device can obtain tissue stiffness quantitatively and independently of operators. Although the designed device is not capable of estimating the tissue stiffness of deep tissue organs, it still provides some encouraging results for the rapid estimation of the stiffness properties of the subcutaneous tissue. Moreover, the control performance of the designed device with large and small target pressures, rather than a single target pressure value, was considered [47], which has implications for the evaluation of future device performance.

Some essential parameters of the proposed LFCA device and existing handheld force-controlled US devices [6], [44], [45], [46], [47] are listed in Table I. The designed LFCA device has significant advantages in terms of mass and length. Conversations with clinical sonographers revealed that prolonged manipulation of the probe by lifting is more likely to cause fatigue than compression. Therefore, when a slight target pressure is required, the designed device avoids the need for lifting, alleviating hand fatigue and facilitating extended US examinations. Despite the small stroke length and low maximum torque of the designed device, the pressure that can be applied to the patient's detection area is sufficient for most US examinations [59]. Moreover, avoiding excessive pressure and stroke lengths contributes to ensuring patient safety. Although not explicitly stated in the literature, the volume and mass of the controller for the designed device are significantly smaller than those designed in [44], [45], [46], and [47].

In addition to the aforementioned advantages of weight and size of the handheld device, other important improvements of this work compared to the previous generation of the device that we have developed in [6] can be highlighted as

TABLE I
COMPARISON OF PARAMETERS FOR THE DESIGNED LFCA DEVICE AND SEVERAL DEVELOPED HANDHELD DEVICES

| Device | Mass (g) | Length (cm) | Diameter (cm) | Usable stroke (cm) | Maximum force (N) |
|---|---|---|---|---|---|
| LFCA | 287 | 14 | 5.1 | 2.5 | 25 |
| [6] | 910 | 17.9 | 6.7 | 5 | 45 |
| [47] | 750 | 15.8 | 5 | 5 | 45 |
| [44], [45] | 850 | 18.5 | 5.4 | 5 | 45 |
| [46] | 1100 | 28 | 7.5 | 10 | 80 |
| [40] | 500 | 200 | 100 | 2 | - |

follows. First, the weight and size of the designed controller are significantly reduced, which remarkably enhances the portability of the device. Second, the control accuracy of the LFCA device is improved with the designed adaptive PID algorithm and error compensation. Third, the ergonomic design of the LFCA device makes the housing easier to hold and more comfortable for sonographers to use for long periods of time. Fourth, the developed rapid tissue stiffness assessment procedure expands the single use of the previous device, thus expanding its application. Fifth, instead of the expensive servo motors in the previous device, a screw-type stepper motor is used (typically less than $12), providing a low-cost advantage that facilitates its widespread application.

### B. Limitations

Despite the potential benefits of the designed LFCA device for US examinations, there are some limitations to its practical use. For example, the cable of the LFCA device may drag across the subject during the examination, causing discomfort. In addition, the size of the LFCA device may still constrain sonographers when performing US scans on children, and the form factor of the device makes it unsuitable for tasks with high inclination angles or requiring frequent rotational scans, such as fetal examinations. However, a device that is too small would not be easy to hold, which remains a widespread problem with handheld US devices.

### C. Evaluation of Safety

The designed LFCA device ensures that excessive pressure is not applied to the end of the probe by limiting the stroke and using a small-thrust motor. Once the pressure applied by the probe to the subject's tissue exceeds 25 N, the probe will stop applying further pressure to the subject to avoid injury to the subject. Different from robotic-assisted US systems, sonographers have absolute control over the handheld device during US examinations, so the power to the controller can be turned off at any time or the device can be moved away from the patient to ensure patient safety. The controller requires only a 5-V operating voltage and 12 V for the motor, and the maximum speed of the device is limited to 17.5 mm/s. Two small fans dissipate the heat to avoid the controller from reaching an excessive temperature when working for an extended period. After a long period of testing, it was found that the designed LFCA device could perform detection tasks continuously for more than 3 h. However, a target pressure of more than 15 N for an hour can cause severe heating of the motor, which should be suspended until the motor temperature returns to normal.

### D. Future Work

The use of software developed by Raspberry Pi makes the LFCA device highly scalable and enables the development of more features than those mentioned in this article, depending on the task requirements. Future work will focus on the following three points. First, we will aim to optimize the LFCA device structure and control system. Bluetooth communication could be used to send and receive control signals, avoiding the influence of the device's cable on US examinations. Second, we will investigate the optimization of the target force. Currently, most force-controlled US devices specify a constant contact force to be applied to the patient. However, the highly deformable properties of human tissue mean that the contact force should be balanced between the requirement for good acoustic coupling and avoiding excessive tissue deformation [24]. In future work, we will establish the relationship between the human tissue characteristics and the target force through a large dataset to achieve more rational adaptive pressure control. Finally, we will consider patient satisfaction when assessing the acceptance of this technology for clinical applications. We strongly believe that handheld US-assisted devices are expected to combine with future advances in other areas, such as artificial intelligence-powered US image analysis, and benefit a wide range of clinical US procedures.

## REFERENCES

[1] H. R. Torres et al., "A review of image processing methods for fetal head and brain analysis in ultrasound images," *Comput. Methods Programs Biomed.*, vol. 215, Mar. 2022, Art. no. 106629.
[2] L. Huang, W. Zhang, and R. Zhang, "Application progress and prospect of ultrasound elastography in clinical staging of deep venous thrombosis," *MEDS Clin. Med.*, vol. 3, no. 2, pp. 30–35, 2022.
[3] U. Walter, "Ultrasound-guided medical procedures: A growing field with new opportunities," *Ultraschall der Medizin-Eur. J. Ultrasound*, vol. 43, no. 4, pp. 327–331, Aug. 2022.
[4] M. Naruse, S. Trappe, and T. A. Trappe, "Human skeletal muscle size with ultrasound imaging: A comprehensive review," *J. Appl. Physiol.*, vol. 132, no. 5, pp. 1267–1279, May 2022.
[5] S. Shah, B. A. Bellows, A. A. Adedipe, J. E. Totten, B. H. Backlund, and D. Sajed, "Perceived barriers in the use of ultrasound in developing countries," *Crit. Ultrasound J.*, vol. 7, no. 1, pp. 1–5, Dec. 2015.
[6] H. Sai, L. Wang, J. Zhang, C. Xia, and Z. Xu, "Portable device to assist with force control in ultrasound acquisition," *IEEE Trans. Ultrason., Ferroelectr., Freq. Control*, early access, Jun. 8, 2022, doi: 10.1109/TUFFC.2022.3181287.
[7] T. Krouskop, T. M. Wheeler, F. Kallel, B. S. Garra, and T. Hall, "Elastic moduli of breast and prostate tissues under compression," *Ultrason. Imag.*, vol. 20, pp. 260–274, Oct. 1998.
[8] D. I. Gendin et al., "Repeatability of linear and nonlinear elastic modulus maps from repeat scans in the breast," *IEEE Trans. Med. Imag.*, vol. 40, no. 2, pp. 748–757, Feb. 2021.
[9] J. Bercoff et al., "In vivo breast tumor detection using transient elastography," *Ultrasound in Med. Biol.*, vol. 29, no. 10, pp. 1387–1396, 2003.
[10] T. Rago, F. Santini, M. Scutari, A. Pinchera, and P. Vitti, "Elastography: New developments in ultrasound for predicting malignancy in thyroid nodules," *J. Clin. Endocrinol. Metabolism*, vol. 92, no. 8, pp. 2917–2922, Aug. 2007.

[11] R. G. Barr and Z. Zhang, "Effects of precompression on elasticity imaging of the breast: Development of a clinically useful semiquantitative method of precompression assessment," *J. Ultrasound Med.*, vol. 31, no. 6, pp. 895–902, Jun. 2012.

[12] H. E. Vanderpool, E. A. Friis, B. S. Smith, and K. L. Harms, "Prevalence of carpal tunnel syndrome and other work-related musculoskeletal problems in cardiac sonographers," *J. Occupational Environ. Med.*, vol. 35, no. 6, pp. 604–610, Jun. 1993.

[13] N. Magnavita, L. Bevilacqua, P. Mirk, A. Fileni, and N. Castellino, "Work-related musculoskeletal complaints in sonologists," *J. Occupational Environ. Med.*, vol. 41, no. 11, pp. 981–988, Nov. 1999.

[14] G. Harrison and A. Harris, "Work-related musculoskeletal disorders in ultrasound: Can you reduce risk?" *Ultrasound*, vol. 23, no. 4, pp. 224–230, Nov. 2015.

[15] M. Muir, P. Hrynkow, R. Chase, D. Boyce, and D. Mclean, "The nature, cause, and extent of occupational musculoskeletal injuries among sonographers: Recommendations for treatment and prevention," *J. Diagnostic Med. Sonography*, vol. 20, no. 5, pp. 317–325, 2004.

[16] M. C. Roshan, A. Pranata, and M. Isaksson, "Robotic ultrasonography for autonomous non-invasive diagnosis—A systematic literature review," *IEEE Trans. Med. Robot. Bionics*, vol. 4, no. 4, pp. 863–874, Nov. 2022.

[17] C. Murphy and A. Russo, "An update on ergonomic issues in sonography," *Healthcare Benefit Trust*, 2000.

[18] W. S. Ng, B. L. Davies, A. G. Timoney, and R. D. Hibberd, "The use of ultrasound in automated prostatectomy," *Med. Biol. Eng. Comput.*, vol. 31, no. 4, pp. 349–354, Jul. 1993.

[19] J. W. Sublett, B. J. Dempsey, and A. C. Weaver, "Design and implementation of a digital teleultrasound system for real-time remote diagnosis," in *Proc. 8th IEEE Symp. Comput.-Based Med. Syst.*, Jun. 1995, pp. 292–298.

[20] S. E. Salcudean, G. Bell, S. Bachmann, W.-H. Zhu, P. Abolmaesumi, and P. D. Lawrence, "Robot-assisted diagnostic ultrasound–design and feasibility experiments," in *Proc. Int. Conf. Med. Image Comput. Comput.-Assist. Intervent.* Springer, 1999, pp. 1062–1071.

[21] F. Pierrot et al., "Hippocrate: A safe robot arm for medical applications with force feedback," *Med. Image Anal.*, vol. 3, no. 3, pp. 285–300, 1999.

[22] E. M. Boctor, M. A. Choti, E. C. Burdette, and R. J. Webster III, "Three-dimensional ultrasound-guided robotic needle placement: An experimental evaluation," *Int. J. Med. Robot. Comput. Assist. Surg.*, vol. 4, no. 2, pp. 180–191, 2008.

[23] T. K. Podder, I. Buzurovic, and Y. Yu, "Multichannel robot for image-guided brachytherapy," in *Proc. IEEE Int. Conf. Bioinf. Bioeng.*, May/Jun. 2010, pp. 209–213.

[24] K. Li, Y. Xu, and M. Q.-H. Meng, "An overview of systems and techniques for autonomous robotic ultrasound acquisitions," *IEEE Trans. Med. Robot. Bionics*, vol. 3, no. 2, pp. 510–524, May 2021.

[25] R. Tsumura and H. Iwata, "Robotic fetal ultrasonography platform with a passive scan mechanism," *Int. J. Comput. Assist. Radiol. Surg.*, vol. 15, no. 8, pp. 1323–1333, Aug. 2020.

[26] M. K. Welleweerd, A. G. de Groot, S. O. H. de Looijer, F. J. Siepel, and S. Stramigioli, "Automated robotic breast ultrasound acquisition using ultrasound feedback," in *Proc. IEEE Int. Conf. Robot. Autom. (ICRA)*, May 2020, pp. 9946–9952.

[27] Q. Huang, B. Wu, J. Lan, and X. Li, "Fully automatic three-dimensional ultrasound imaging based on conventional B-scan," *IEEE Trans. Biomed. Circuits Syst.*, vol. 12, no. 2, pp. 426–436, Apr. 2018.

[28] P. Chatelain, A. Krupa, and N. Navab, "Confidence-driven control of an ultrasound probe," *IEEE Trans. Robot.*, vol. 33, no. 6, pp. 1410–1424, Dec. 2017.

[29] Z. Jiang, M. Grimm, M. Zhou, Y. Hu, J. Esteban, and N. Navab, "Automatic force-based probe positioning for precise robotic ultrasound acquisition," *IEEE Trans. Ind. Electron.*, vol. 68, no. 11, pp. 11200–11211, Nov. 2021.

[30] A. S. B. Mustafa et al., "Development of robotic system for autonomous liver screening using ultrasound scanning device," in *Proc. IEEE Int. Conf. Robot. Biomimetics (ROBIO)*, Dec. 2013, pp. 804–809.

[31] S. Merouche, L. Allard, E. Montagnon, G. Soulez, P. Bigras, and G. Cloutier, "A robotic ultrasound scanner for automatic vessel tracking and three-dimensional reconstruction of B-mode images," *IEEE Trans. Ultrason., Ferroelectr, Freq. Control*, vol. 63, no. 1, pp. 35–46, Jan. 2016.

[32] C. Hennersperger et al., "Towards MRI-based autonomous robotic U.S. Acquisitions: A first feasibility study," *IEEE Trans. Med. Imag.*, vol. 36, no. 2, pp. 538–548, Feb. 2017.

[33] J. Zhan, J. Cartucho, and S. Giannarou, "Autonomous tissue scanning under free-form motion for intraoperative tissue characterisation," in *Proc. IEEE Int. Conf. Robot. Automat. (ICRA)*, May/Aug. 2020, pp. 11147–11154.

[34] S. E. Salcudean, H. Moradi, D. G. Black, and N. Navab, "Robot-assisted medical imaging: A review," *Proc. IEEE*, vol. 110, no. 7, pp. 951–967, Jul. 2022.

[35] D. R. Swerdlow, K. Cleary, E. Wilson, B. Azizi-Koutenaei, and R. Monfaredi, "Robotic arm–assisted sonography: Review of technical developments and potential clinical applications," *Amer. J. Roentgenol.*, vol. 208, no. 4, pp. 733–738, 2017.

[36] M. R. Burcher, J. A. Noble, L. Man, and M. Gooding, "A system for simultaneously measuring contact force, ultrasound, and position information for use in force-based correction of freehand scanning," *IEEE Trans. Ultrason., Ferroelectr, Freq. Control*, vol. 52, no. 8, pp. 1330–1342, Aug. 2005.

[37] T. Schimmoeller et al., "Instrumentation of off-the-shelf ultrasound system for measurement of probe forces during freehand imaging," *J. Biomech.*, vol. 83, pp. 117–124, Jan. 2019.

[38] M. W. Gilbertson and B. W. Anthony, "An ergonomic, instrumented ultrasound probe for 6-axis force/torque measurement," in *Proc. 35th Annu. Int. Conf. IEEE Eng. Med. Biol. Soc. (EMBC)*, Jul. 2013, pp. 140–143.

[39] M. Dhyani et al., "A pilot study to precisely quantify forces applied by sonographers while scanning: A step toward reducing ergonomic injury," *Work*, vol. 58, no. 2, pp. 241–247, 2017.

[40] F. Eura, R. Aizawa, R. Kondo, K. Tomita, Y. Nishiyama, and N. Koizumi, "Development of portable ultrasound guided physiological motion compensation device," in *Proc. IEEE Int. Conf. Cyborg Bionic Syst. (CBS)*, Oct. 2017, pp. 243–247.

[41] M. Marchal and J. Troccaz, "A one-DOF free-hand haptic device for robotic tele-echography," in *Studies in Health Technology and Informatic*, Newport Beach, CA, USA, 2004, pp. 231–233.

[42] A. Nabavizadeh et al., "Automated compression device for viscoelasticity imaging," *IEEE Trans. Biomed. Eng.*, vol. 64, no. 7, pp. 1535–1546, Jul. 2017.

[43] N. Wah and M. T. S. Aung, "Proxy based sliding mode control augmented with friction compensator for use in 1-DOF freehand ultrasound probe," in *Proc. 43rd Annu. Conf. IEEE Ind. Electron. Soc. (IECON)*, Oct. 2017, pp. 2911–2916.

[44] M. W. Gilbertson and B. W. Anthony, "Ergonomic control strategies for a handheld force-controlled ultrasound probe," in *Proc. IEEE/RSJ Int. Conf. Intell. Robots Syst.*, Oct. 2012, pp. 1284–1291.

[45] M. W. Gilbertson and B. W. Anthony, "Force and position control system for freehand ultrasound," *IEEE Trans. Robot.*, vol. 31, no. 4, pp. 835–849, Aug. 2015.

[46] S. Koppaka, M. W. Gilbertson, S. B. Rutkove, and B. W. Anthony, "Evaluating the clinical relevance of force-correlated ultrasound," in *Proc. IEEE 11th Int. Symp. Biomed. Imag. (ISBI)*, Apr. 2014, pp. 1172–1175.

[47] M. W. Gilbertson and B. W. Anthony, "Impedance-controlled ultrasound probe," *Proc. SPIE*, vol. 7968, pp. 348–359, Mar. 2011.

[48] S. Koppaka, M. W. Gilbertson, J. S. Wu, S. B. Rutkove, and B. W. Anthony, "Assessing Duchenne muscular dystrophy with force-controlled ultrasound," in *Proc. IEEE 11th Int. Symp. Biomed. Imag. (ISBI)*, Apr. 2014, pp. 694–697.

[49] H. Rivaz and R. Rohling, "An active dynamic vibration absorber for a hand-held vibro-elastography probe," *J. Vibrat. Acoust.*, vol. 129, no. 1, pp. 101–112, Feb. 2007.

[50] M. W. Gilbertson, "Electromechanical systems to enhance the usability and diagnostic capabilities of ultrasound imaging," Ph.D. dissertation, Dept. Mech. Eng., Massachusetts Inst. Technol., Cambridge, MA, USA, 2014.

[51] M. Dhyani et al., "Ultrasound shear wave elastography: Variations of liver fibrosis assessment as a function of depth, force and distance from central axis of the transducer with a comparison of different systems," *Ultrasound Med. Biol.*, vol. 44, no. 11, pp. 2209–2222, 2018.

[52] L. A. Wood, C. W. Suggs, and C. F. Abrams, "Hand-arm vibration Part III: A distributed parameter dynamic model of the human hand-arm system," *J. Sound Vib.*, vol. 57, no. 2, pp. 157–169, Mar. 1978.

[53] J. E. Speich, L. Shao, and M. Goldfarb, "Modeling the human hand as it interacts with a telemanipulation system," *Mechatronics*, vol. 15, no. 9, pp. 1127–1142, Nov. 2005.

[54] S. Ødegaard, M. B. Kimmey, R. W. Martin, H. C. Yee, A. H. S. Cheung, and F. E. Silverstein, "The effects of applied pressure on the thickness, layers, and echogenicity of gastrointestinal wall ultrasound images," *Gastrointestinal Endoscopy*, vol. 38, no. 3, pp. 351–356, May 1992.

[55] R. G. Lyons, *Understanding Digital Signal Processing*, 3rd ed. London, U.K.: Pearson, 1997.
[56] K. H. Lee, H. J. Lee, J. Lee, S.-H. Ji, and J. C. Koo, "A simple method to estimate the impedance of the human hand for physical human–robot interaction," in *Proc. 14th Int. Conf. Ubiquitous Robots Ambient Intell. (URAI)*, Jun. 2017, pp. 152–154.
[57] J. Zhang, Y. Wang, T. Liu, K. Yang, and H. Jin, "A flexible ultrasound scanning system for minimally invasive spinal surgery navigation," *IEEE Trans. Med. Robot. Bionics*, vol. 3, no. 2, pp. 426–435, May 2021.
[58] N. Bogduk, "Functional anatomy of the spine," in *Handbook of Clinical Neurology*, vol. 136. 2016, pp. 675–688.
[59] N. Smith-Guerin, L. Al Bassit, G. Poisson, C. Delgorge, P. Arbeille, and P. Vieyres, "Clinical validation of a mobile patient-expert teleechography system using ISDN lines," in *Proc. 4th Int. IEEE EMBS Special Topic Conf. Inf. Technol. Appl. Biomed.*, Apr. 2003, pp. 23–26.

**Huayang Sai** received the B.E. degree from the School of Mechanical and Electronic Engineering, Northwest A&F University, Xianyang, China, in 2018. He is currently pursuing the Ph.D. degree in mechanical engineering and automation with the Changchun Institute of Optics, Fine Mechanics and Physics, Chinese Academy of Science, Changchun, China, and the Ph.D. degree with the College of Optoelectronics, University of Chinese Academy of Sciences, Beijing, China.

His current research interests include medical robots and dynamic control of robots.

**Zhenbang Xu** received the B.E. degree from the Department of Theoretical and Applied Mechanics, Chinese Academy of Sciences University, Hefei, China, in 2005, and the Ph.D. degree from the Chinese Academy of Sciences University in 2010, where he is currently with the Changchun Institute of Optics, Fine Mechanics and Physics.

His research interests include space intelligent robots, multidimensional precision adjustment mechanisms, space structure dynamics, and microvibration control.

**Chengkai Xia** received the B.E. degree from the School of Engineering Science, University of Science and Technology of China, Hefei, Anhui, China, in 2019. He is currently pursuing the Ph.D. degree in mechanical engineering and automation with the Changchun Institute of Optics, Fine Mechanics and Physics, Chinese Academy of Science, Changchun, China, and the degree with the College of Optoelectronics, University of Chinese Academy of Sciences, Beijing, China.

His current research interests include the design, modeling, and control of soft robots.

**Lijuan Wang** received the M.D. and Ph.D. degrees from the Department of Neurology, The First Hospital of Jilin University, Jilin University, Changchun, China, in 2006 and 2015, respectively.

She was a Visiting Scholar with the Prince of Wales Hospital, The Chinese University of Hong Kong, Hong Kong, from 2012 to 2013. She currently works at the Department of Neurovascular Ultrasonography, The First Hospital of Jilin University. Her research interests include ultrasonic diagnosis of nervous system diseases, ocular diseases, and vascular diseases.

**Jie Zhang** received the M.D. and Ph.D. degrees from the Department of Neurology, The First Hospital of Jilin University, Jilin University, Changchun, China, in 2010 and 2022, respectively.

She currently works at the Department of Neurovascular Ultrasonography, The First Hospital of Jilin University. Her research interests include ultrasonic diagnosis of nervous system diseases and vascular diseases.